Coverage induced regulation of Au nanoparticles during pulsed laser deposition

V. Resta,[1,a)] J. Gonzalo,[1] C. N. Afonso,[1] E. Piscopiello,[2] and J. García López[3]
[1]*Laser Processing Group, Instituto de Optica, CSIC, Serrano 121, E-28006 Madrid, Spain*
[2]*Unità Tecnica Tecnologie dei Materiali Brindisi (UTTMATB), Strada Statale 7 "Appia"—Km 706*
[3]*Centro Nacional de Aceleradores, Universidad de Sevilla/CSIC, T.A. Edison, Isla de la Cartuja E-41092, Spain*

(Received 19 May 2010; accepted 15 December 2010; published online 2 May 2011)

The effects induced during the covering/embedding of metal nanoparticles (NPs) produced by pulsed laser deposition (PLD) and their impact on the structural and optical properties have been studied by producing pairs of samples containing Au NPs that are either uncovered (i.e., at the surface) or covered (i.e., embedded in an amorphous a-Al_2O_3 host). The main result is that covering species can sputter up to 100% of the Au atoms, the smaller the NPs the higher the sputtered fraction. This fraction has been simulated using standard models for ion bombardment and taking into account the kinetic energy distribution of arriving species and the cohesive energy dependence on NPs dimensions. Although all models well predict the order of magnitude of the sputtering yield, the calculated values are generally smaller than the experimental ones and do not account for the experimental dependence on NPs dimensions. This disagreement is discussed in terms of the limitations of standard models that do not take into account the lower adhesion of small NPs to the substrate, the high flux of species involved in PLD and, possibly to lesser extent, the use of some bulk material parameters. The metal sputtering during the coverage regulates the NPs morphology, through a reduction of dimensions and dimension dispersion. Most changes of structural features and optical spectra when covering the NPs are directly related to the variation in the amount of metal with the exception of a strong blueshift of the surface plasmon resonance when NPs are covered. This shift could be consistent with mixing of covering layer species and metal at the surface of the NPs. © *2011 American Institute of Physics*. [doi:10.1063/1.3549168]

I. INTRODUCTION

The unique optical properties of metal nanoparticles (NPs) give rise to a broad range of possible applications in linear optics, such as polarizers,[1] and filters,[2] as well as in information technology, such as data storage devices, [3,4] or all-optical ultrafast switching.[5–7] The optical response is characterized by an absorption band related to the surface plasmon resonance (SPR).[8,9] While the SPR lies in the UV region for most metals, it lies in the visible region for Au, Ag, or Cu, the specific position of the SPR depending on the NPs size and shape.[10]

For most applications in optics or information technologies, NPs should be embedded in a solid media. The most versatile approach is the use of thin film technologies for producing both the metal NPs and the embedding/covering layer. Pulsed laser deposition (PLD) has successfully been used to produce such embedded metal NPs in an oxide host and having narrow size distributions. It is well established that this technique involves high kinetic energy species. Several works have reported the production of shallow implantation, self-sputtering and backscattering of metal atoms and found that self-sputtering of Fe, Ag, or Au increases with increasing laser fluence.[11–13] For the case of Au,[14] it has also been observed self-sputtering of 60%–70% of the species arriving to the substrate for ablation fluences in the range 2.7–9.0 J cm^{-2}, due to gold ions with kinetic energies >200 eV. Instead, the implications of sputtering during the covering process have much less been studied. It has been reported that the competition between surface growth and sputtering at high fluences leads to self-regulation of the dimensions of embedded NPs that narrows the size distributions,[13] and when using high fluences to ablate the Al_2O_3 host, it leads to a reshaping of the and even to an elongation in the growth direction.[15] It is, in addition, suggested that sputtering by the host depends on the size of the NPs.

This work aims to quantify the metal sputtered during deposition of the covering/embedding layer and to understand its effect on the morphology and optical properties as a function of the metal content, i.e., NPs dimensions and coverage. The system formed by Au NPs embedded in an amorphous a-Al_2O_3 layer has been selected because earlier works have already shown that covering with this host modifies the NPs morphology[13,15] and thus direct comparison is possible. A novel approach comparing pairs of samples containing uncovered and covered metal NPs has been used that provides direct experimental values of the amount of sputtered metal during the cover process.

II. EXPERIMENTAL PROCEDURES

The samples have been produced by alternate PLD in vacuum (5×10^{-6} mbar) by focusing an ArF laser beam [$\lambda = 193$ nm, $\tau = 20$ ns full-width half-maximum (FWHM)]

[a)]Present address: ENEA, Unità Tecnica Tecnologie dei Materiali Brindisi (UTTMATB), Strada Statale 7 "Appia"-Km 706, I-72100 Brindisi, Italy. Electronic-mail: vincenzo.resta@enea.it.

on bulk Al_2O_3 and Au targets at an angle of 45° with respect to its normal. The laser repetition rate has been set at 20 Hz and the fluence at the target site at ~ 2.7 J cm^{-2}. The substrate was held at room temperature and placed 40 mm away from the target. Further details on the deposition procedure can be found elsewhere.[13]

Due to the high directionality of the plasma expansion produced by laser ablation, the deposit is homogenous (within <5%) in a reduced area ($\approx 5 \times 3$ mm^2) around the center of the plasma. All results reported in the present work relate to data obtained from this area. Deposition was performed simultaneously on three types of substrates: a 1-mm-thick glass plate, a Si wafer and a carbon-coated mica substrate. A 10-nm-thick *a*-Al_2O_3 buffer layer has always been produced before the ablation of the gold target in order to provide the same nucleation surface, regardless of the substrate used. The number of pulses used to ablate the gold target has been varied in order to change the gold coverage. For each gold coverage, a pair of samples has been produced. One of them, referred to as *on* sample, is produced by depositing gold on the *a*-Al_2O_3 buffer leading to Au NPs that are uncovered. The second one, referred to as *in* sample, is produced first as the corresponding *on* sample and then covered by a 10 nm thick layer of *a*-Al_2O_3, thus leading to NPs embedded in this medium.

The gold content [Au] has been measured in the specimens produced on Si substrates, by Rutherford backscattering using a 3 MeV proton beam and the spectra have been analyzed with the SENRAS code, the error determination of the gold content being 2%. The morphology of the Au NPs has been characterized by transmission electron microscopy (TEM). Plan-view specimens have been prepared by floating off the films from the carbon-coated mica substrate in de-ionized water and picking them up on copper grids for observation. TEM observations have been performed using a TECNAI F30 TEM operating at 300 kV and point-to-point resolution of 0.205 nm. The image analysis has been performed by studying areas of at least 200×200 nm^2 by means of the software *ImageJ*.[16] Using the free hand tool, we manually outlined the NPs to produce a binary image in which the NPs appear black against a white background. The NP diameter is finally determined by averaging the measured length *l* (the longer in-plane dimension) and width *w* (the in-plane dimension perpendicular to *l*) in the binary images.

Finally, the optical extinction spectra of the specimens produced on glass substrates have been calculated as $\ln(1/T)$, where T is the transmission measured at 0° of incidence angle with unpolarized light in the range 400–800 nm using a spectroscopic ellipsometer (WVase).

III. RESULTS

Figure 1 shows the evolution of [Au] measured in both *on* ($[Au]_{on}$) and *in* ($[Au]_{in}$) samples as a function of the number of pulses used to ablate the gold target. Both $[Au]_{on}$ and $[Au]_{in}$ increase with the number of pulses, the former being always higher than the latter and the difference being nearly constant ($\approx 4.0 \times 10^{15}$ atoms cm^{-2}) for a number of pulses >350.

Figure 2 shows TEM images of a pair of *on* (a) and *in* (b) samples, i.e., produced with the same number of pulses (640)

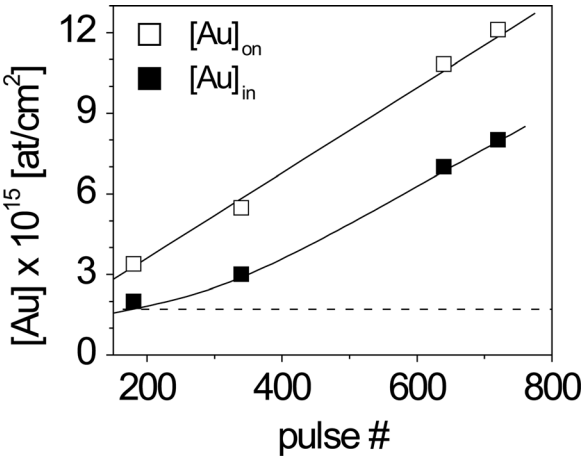

FIG. 1. Gold content of *on* (□) and *in* (■) samples as a function of the number of laser pulses used to ablate the gold target. The dashed line indicates the gold threshold for the formation of NPs at the surface taken from Ref. 13. Full lines are guidelines.

in the metal target. The images show in all cases dark areas corresponding to the metal NPs. They evidence a bimodal distribution of small and large NPs that were shown in an earlier work[13] to be respectively related to NPs produced by the implantation of the metal in the substrate and to NPs nucleated at the surface. It was reported that gold threshold for the formation of NPs at the surface is $2.1 \pm 0.2 \times 10^{15}$ at. cm^{-2} and

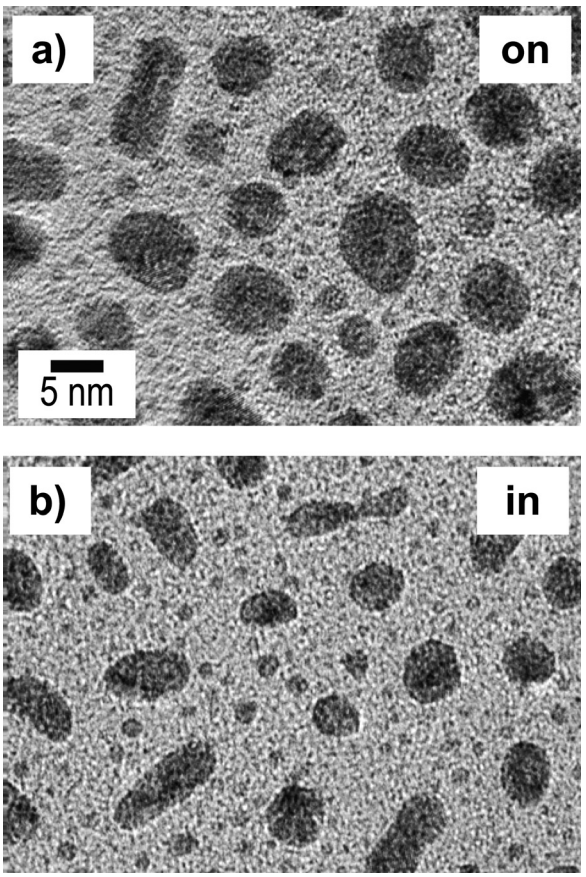

FIG. 2. TEM images of a pair of *on* (a) and *in* (b) samples produced using 640 laser pulses on the gold target and having, respectively, metal contents of 11.0×10^{15} atoms cm^{-2} (a) and 7.0×10^{15} atoms cm^{-2} (b).

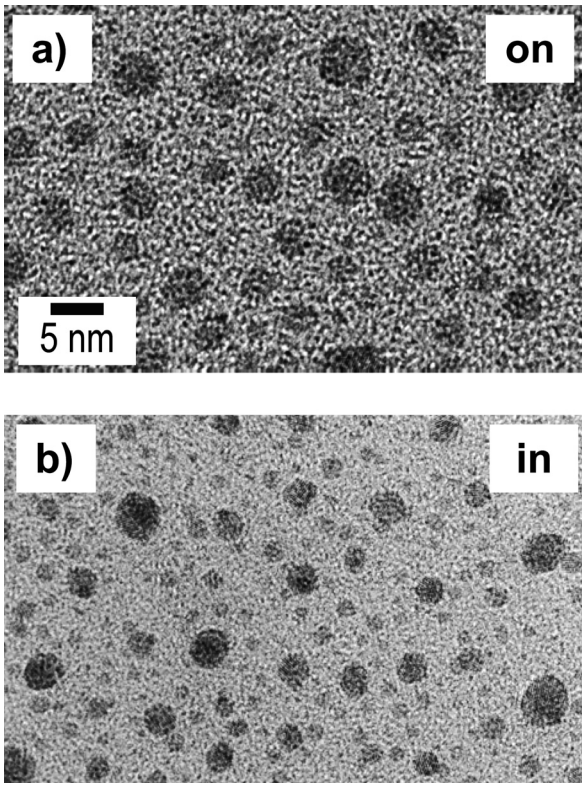

FIG. 3. TEM images of *on* sample with $[Au]_{on} = 5.5 \times 10^{15}$ at. cm^{-2} (a) and *in* sample with $[Au]_{in} = 4.9 \times 10^{15}$ at. cm^{-2} (b). Figure 3(b) is reprinted with permission from J. Gonzalo, A. Perea, D. Babonneau, C.N. Afonso, N. Beer, J.-P. Barnes, A.K. Petford-Long, K.E. Hole and P.D. Townsend; Phys. Rev. B 71, 125420 (2005). © (2011) by the American Physical Society. (http://prb.aps.org/abstract/PRB/v71/i12/e125420).

smaller values lead to NPs below the surface by implantation of 1.4±0.5 nm size.[13] This gold content is indicated in Fig. 1 as a dashed line. The comparison of large NPs of *on* to *in* samples clearly shows that the latter are significantly smaller than the former, this result appears to be consistent with the lower $[Au]_{in}$ as seen in Fig. 1. From now on, the results and discussion will refer to the large NPs only and the small NPs will be referred to as implanted ones.

Figure 3(a) shows a TEM image of an *on* sample produced in this work using 340 pulses and having a metal content of $[Au]_{on} = 5.5 \times 10^{15}$ atoms cm^{-2}, whereas Fig. 3(b) shows a TEM image of an *in* sample taken from Ref. 13 that was produced under similar conditions than in the present work and having a similar metal content ($[Au]_{in} = 4.9 \times 10^{15}$ atoms cm^{-2}). The comparison of these images shows that both samples have nearly round like NPs.

The NP diameter obtained from TEM images is shown as a function of the metal content in Fig. 4 where the dashed area refers to the implanted NPs according to Ref. 13. The results show that the mean diameter increases linearly with the metal content, this result thus highlighting that the mean diameter is determined by the effective [Au] irrespective of the NPs being covered or uncovered. It is worth pointing out that the dispersion of mean diameter (error bars in Fig. 4) is generally smaller for *in* than *on* samples.

The extinction spectra of different *on* (full lines) and *in* (dashed lines) samples are presented in Fig. 5 showing a blue

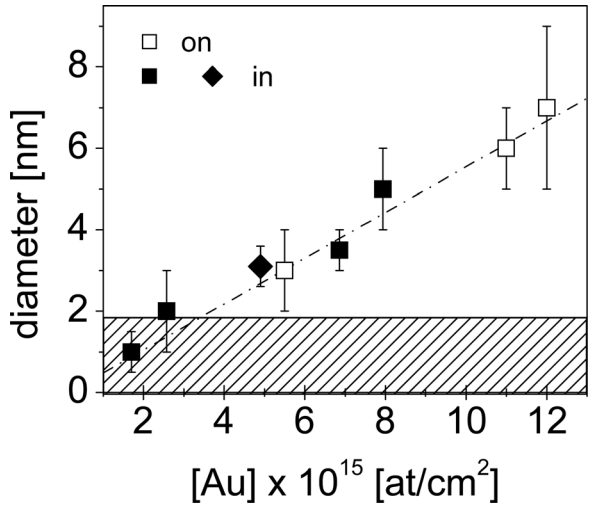

FIG. 4. Evolution of the mean diameter of NPs as a function of the metal content of both *on* (□) and *in* (■,◆) samples. The filled square (■) refers to samples produced in this work, while the filled diamond (◆) and the dashed region correspond, respectively, to the sample whose image is shown in Fig. 3(b) and to implanted NPs, both taken from Ref. 13. The dash–dot line is a linear fit of the experimental data and error bars are dispersion of the data.

shift of the SPR as $[Au]_{on}$ decreases. Similarly, the SPR blueshifts when covering the NPs, as evidenced when comparing the spectra of pairs of *in* and *on* samples, see for instance those labeled 12.0 and 8.0. Finally, the SPR is not seen for $[Au] \leq 3.4 \times 10^{15}$ atoms cm^{-2}, irrespective of the sample being *in* or *on*, in spite of the TEM images evidence the samples contain small metal NPs (see Fig. 4). The wavelength and extinction of the SPR for all samples are summarized in Fig. 6 as a function of the gold content where the dashed area represents the interval in which no SPR is seen in the spectra even when the formation of NPs is observed. The results show that both wavelength and extinction at the SPR increase as the metal content is increased. The extinction fits well within a linear trend, irrespective of the NPs being covered or uncovered. Instead, the SPR wavelength dependence with metal content appears more pronounced for *in* than *on*

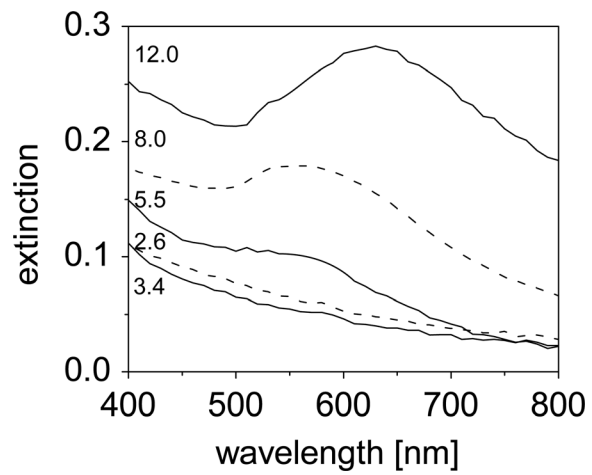

FIG. 5. Extinction spectra of *on* (full lines labeled 3.4, 5.5, 12) and *in* (dashed lines labeled 2.6, 8.0) samples. The labels are the gold content of the specimens ($\times 10^{-15}$ atoms cm^{-2}) that were produced using 180 (3.4), 340 (5.5 and 2.6), and 720 (12.0 and 8.0) laser pulses on the gold target.

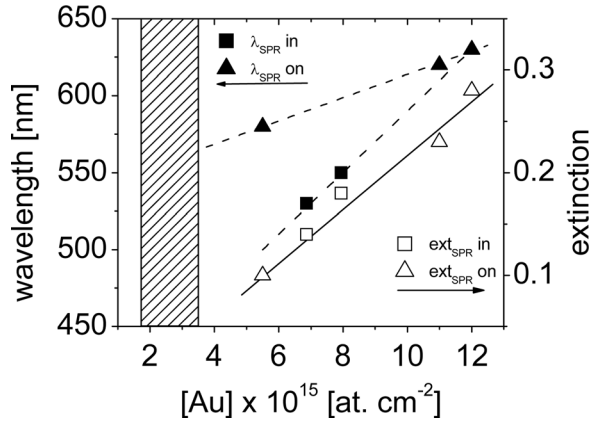

FIG. 6. Wavelength (■,▲) and extinction (□,Δ) at the SPR of *on* (▲,Δ) and *in* (■,□) samples as a function of the metal content. The dashed region corresponds to samples in which no SPR is detected. Lines are linear fits of the experimental data.

samples, the former samples showing a SPR shifted to the blue as described earlier at least for small NPs.

IV. DISCUSSION

The results clearly show that the covering process has important consequences on the metal content retained at the substrate and eventually a direct impact on the NPs morphology and optical properties. Fig. 1 evidences there is a strong sputtering of the metal species when producing the covering layer. Since $[Au]_{on}$ represents the metal content of $[Au]_{in}$ before covering the NPs with a-Al_2O_3, the difference $[Au]_{on}-[Au]_{in}$ directly provides the amount of Au sputtered during the covering process. In calculating the sputtering fraction $([Au]_{on}-[Au]_{in})/[Au]_{on}$ one has to take into account that only NPs at the surface can be sputtered and therefore, the amount of metal implanted has to be extracted in all metal contents. Since the threshold reported elsewhere[13] for surface nucleation was $2.1\pm0.2\times10^{15}$ at. cm^{-2} and

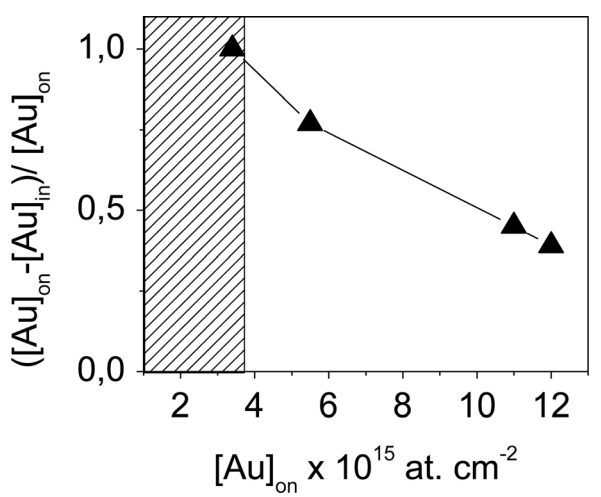

FIG. 7. Experimentally determined gold sputtered fraction as a function of the total initial number of gold atoms $[Au]_{on}$. Line is a guideline and the dashed region provides the $[Au]_{on}$ range that leads to no surface formation of NPs for *in* samples.

1.7×10^{15} at. cm^{-2} was the gold content of the only sample having a gold value below that threshold, we have assumed that this is the gold content of the implanted layer in all cases. The results are plotted in Fig. 7 and show that the sputtered fraction increases as the metal content consistent with its gold content. decreases reaching 100% for the sample with the lowest metal content consistent with its gold content. The diameter of the NPs in this *in* sample was 1.0 ± 0.5 nm (Fig. 4), which is consistent with all the NPs being produced by implantation before the covering process.[13] The vertical dashed area in Fig. 7 thus marks a minimum metal content range for *on* samples that leads to no-surface nucleation because all surface metal is sputtered during the covering process.

During ion bombardment, when the energy transferred from the arriving species or projectiles becomes of the order of the cohesive energy, the rupture of chemical bonds of the lying species leads to enhanced sputtering. The cohesive energy is a constant for bulk materials,[17] but becomes size dependent for NPs because the lower coordination number of surface atoms makes them less stable than inside atoms.[18,19] The cohesive energy of small NPs decreases as their size decreases according to the following relation:

$$E_{CNP} = E_{CB}(1 - 3\alpha/4), \quad (1)$$

where E_{CNP} and E_{CB} are, respectively, the cohesive energy of the NP and the bulk material, $\alpha = 3d/R$ is the surface-to-volume atomic ratio for spherical NPs, d is the atomic diameter, and $2R$ is the NP diameter.[18] Table I summarizes the cohesive energy of NPs in two samples studied in this work that were estimated using this approach and $E_{CB} = 3.8$ eV for bulk gold together with the main experimental data for these samples.

The kinetic energy (KE) of arriving species is an essential parameter in order to calculate the sputtering yield (Y) defined as the number of atoms sputtered away from the substrate per projectile. It is widely reported that PLD involves high KE species and, in an earlier work, we have shown the importance of using the actual KE energy distribution rather than the mean KE value in order to make a proper evaluation of the extent of the sputtering process.[14] Experiments performed by laser induced fluorescence on plasmas generated by laser ablation of Al_2O_3 report on the existence of Al and AlO species.[20] However, whereas the mean KE of Al species increases with fluence (up to 20 eV at 3 J cm^{-2}), that of AlO decreases and thus their impact on substrate bombardment is neglected. In addition, Langmuir probe measurements upon ablation of Al targets have shown that the plasma dynamics is dominated by Al^+ rather than by neutrals, the KEs of the former being up to 100 times higher than those of the latter.[21] We can thus assume that sputtering during the coverage process is dominated by Al^+ bombardment and use the KE distribution reported elsewhere for 2.5 J cm^{-2} as characteristic of the incident species responsible for Au sputtering.[21]

The amount of sputtered Au atoms $[Au]_{SPUTT}$ has first been calculated using the SRIM-2008 software[22,23] following the procedure described in the Appendix. The results achieved for the two samples for which calculations were

TABLE I. Number of pulses used to produce the sample, experimental number of sputtered metal atoms ($[Au]_{on}$–$[Au]_{in}$), diameter of NPs and film coverage (Cov.) in the *on* sample, cohesive energy of NPs calculated using the approach in Ref. 18, and calculated number of metal atoms sputtered $[Au]_{SPUTT}$ using the SRIM,[a] Zalm,[b] and Yamamura and Tawara[c] models.

Number of pulses	$[Au]_{on}-[Au]_{in}$ ($\times 10^{15}$ atoms cm^{-2})	NP diameter (nm)	Cov. (%)	E_{CNP} (eV)	$[Au]_{SPUTT\ SRIM}$ ($\times 10^{15}$ atoms cm^{-2})	$[Au]_{SPUTT\ ZALM}$ ($\times 10^{15}$ atoms cm^{-2})	$[Au]_{SPUTT\ YAMAMURA}$ ($\times 10^{15}$ atoms cm^{-2})
340	2.9 ± 0.2	3 ± 1	25 ± 12	2.16	0.8 ± 0.4	1.0 ± 0.5	1.6 ± 0.7
720	4.1 ± 0.5	7 ± 2	41 ± 9	3.1	1.0 ± 0.2	1.0 ± 0.2	1.6 ± 0.7

[a]References 22 and 23.
[b]Reference 25.
[c]Reference 26.

performed are included in Table I, where it is seen that $[Au]_{SPUTT}$ is of the same order of magnitude as the experimental ones but significantly lower (factor 2–4). The reliability of SRIM software reported elsewhere could be relevant in our case as the atomic number of the projectile is significantly lower than that of the target.[24] According to this report, $[Au]_{SPUTT}$ would be overestimated by a factor of ~ 2 as $Z_{Al}^{+}/Z_{Au} < 0.7$, this yielding to $[Au]_{SPUTT}$ values even smaller than those included in Table I. Thus, we have explored the use of other models, namely those reported by Zalm[25] and Yamamura and Tawara,[26] in order to find a more accurate fit to the experimental values as described in the Appendix. The results are also included in Table I where it is seen that even the higher values calculated with the model of Yamamura and Tawara are still lower than the experimental ones except for the sample having the smallest gold content. The value calculated for the sample having the largest gold content is still more than two times smaller. Irrespective of the model used, the same $[Au]_{SPUTT}$ value is achieved within the error for the two samples, i.e., no dependence on NPs dimensions is predicted. This unexpected result appears to be related to the opposite effects of the coverage and cohesive energy as a function of the NPs dimensions that somehow compensate each other.

The main conclusion is that the calculations provide the order of magnitude of the sputtering yield but not the actual values. There are several approximations and limitations in the calculations and models considered that deserve to be mentioned. First, while the dependence of the cohesive energy of metal on dimensions of NPs has been taken into account, bulk values have been used for displacement and lattice binding energies of gold. Second, we have considered that sputtering is only caused by Al^{+}, but there can be other ions having significant kinetic energies ($\geq$200 eV), such as higher ionized species. However, their number is generally considered negligible with respect to that of single ionized ones. Third, the decrease of strength of the bond between clusters and substrate below a critical size[27]or the role of energy spike effects caused by spatial confinement in the NPs[28] is not taken into account. Last but not least, time is not an important parameter in the standard models used, whereas the arrival of ions in PLD using nanosecond laser pulses occurs in a short time interval (typically <10 μs).[14] The very high flux involved in PLD compared to that in standard ion bombardment processes for which the considered models have been developed can be an extra parameter playing an important role.

Figures 2–4 show that the main consequences of the sputtering during the coverage are the reduction of NPs in-plane dimensions and dimension dispersion. The overall in-plane mean diameter of the NPs follow a linear dependence on the metal content irrespective that they are on the surface or embedded. Also, the optical spectra (Fig. 5) of covered Au NPs are generally consistent with their smaller dimensions with respect to uncovered ones. The covering process decreases the extinction intensity at the SPR consistently with the reduction of the metal NPs dimensions and their dimension dispersion. For samples with $[Au] \leq 3.4 \times 10^{15}$ at. cm^{-2}, the SPR is not seen irrespective that the NPs are *on* or *in* is most likely related to the dimensions of the NPs being below the threshold for having enough electrons contributing to collective oscillations.[5] The significant shift to the blue of the SPR seen in Fig. 6 of an *in* sample with respect to an *on* sample having similar gold content is more intriguing. On the one hand, the reduced dimension dispersion when NPs become covered can account for some blueshift of the SPR. On the other hand, the existence of mixing processes between host and metal species at the NPs surface reported elsewhere for Cu NPs embedded in a-Al_2O_3 can provide additional contribution to this shift.[29] This mixing process would modify the surface of the NPs, making the actual mean diameter of the metallic core contributing to the SPR smaller than the one measured from TEM images. At the intermediate energy density used in the present work to ablate the Al_2O_3 target, this process is expected to be relevant only for small NPs consistently with the expected trend deduced from Fig. 6.

V. CONCLUSIONS

The covering process of metal NPs has important consequences on the final features and optical properties of the embedded NPs. These consequences are mainly related to the sputtering of metal by covering layer species that can be as high as 100%, the smaller the NPs the higher the sputtering fraction. Standard models for ion bombardment combined with PLD kinetic energy distribution of arriving Al^{+} and cohesive energy dependence on NPs dimensions predict the order of magnitude of the sputtering yield. However, the calculated values are generally smaller than the experimental ones and do not predict the experimental dependence on NPs dimensions. This disagreement is most likely related to the limitations of the standard models that do not take into account the lower adhesion of small NPs to the substrate and the high flux of species involved in PLD, as well as the use

of bulk values for displacement and lattice binding energies of gold. Overall, the sputtering process during the covering process leads to a regulation of the dimensions of the NPs, namely a reduction of their dimensions and dimension dispersion. The detailed analysis of these parameters allows us to conclude that the NPs dimensions are mainly determined by the final metal content remaining at the surface. The shift to the blue of the SPR of covered NPs with respect to uncovered ones suggest that mixing between metal and covering layer species might be playing a role especially for small NPs.

ACKNOWLEDGMENTS

This work was partially supported by MAT2009-14282-C02-01 (Spain). We thank M.M.N.R. Ashfold and F. Claeyssens from Bristol University for providing the kinetic energy distribution of Al^+ ions at 2.5 J cm^{-2}, as well as making us aware of the error in Fig. 2 of Ref. 21 related to the assignment of data to Al.

APPENDIX

The amount of sputtered Au atoms per pulse $[Au]_{SPUTT}$/pulse by energetic species reaching the substrate during the covering process with *a*-Al_2O_3 has first been calculated using the SRIM-2008 software:[22,23]

$$[Au]_{SPUTT}/\text{pulse} = \int QN(E)Y(E)dE, \qquad \text{(A1)}$$

where Q is the integrated ion density, $N(E)$ is the normalized KE distribution of incident species per pulse, and $Y(E)$ is the KE-dependent sputtering yield of Au. In order to determine the values of $Y(E)$, we have used the parameters of bulk Au for the density (19.11 g cm^{-3}), lattice binding energy (3.0 eV), and displacement energy (25 eV).[11,12,22] As characteristic cohesive energy, we have used those values determined using Eq. (1) for the NP dimensions that are listed in Table I.

As discussed in the main text, we consider Al^+ ions as the ones contributing to the process and assume they arrive perpendicular to the surface substrate due to the strongly forward peaked character of the laser ablation generated plasma[30] and the fact that the studies are performed in a reduced region around the center of the plasma. We use the KE distribution reported elsewhere[21] for Al^+ ions upon ablation of Al at 2.5 J cm^{-2} and an integrated ion density of $Q = 3.2 \times 10^{15}$ ions cm^{-2} pulse. The fact that the metal is forming NPs rather than a continuous layer has led to two approximations. The first one relates to the incident angle of Al^+ ions with respect to the surface of Au NPs, which can vary from 0° to 90° with respect to the substrate surface normal. We have evaluated the effect of the angle of incidence on $Y(E)$ of Au for incident Al^+ ions having KE's in the range of 50–800 eV, which corresponds, respectively, to the threshold to observe sputtering and to the maximum value of the above-mentioned KE distribution. Since the results achieved as a function of the incidence angle are higher or smaller than those at normal incidence by a factor of 8% at most, we have considered normal incidence for Al^+ ions in the calculations. In practice, this means that the shape of the NPs are approximated to cylindroids having their axis perpendicular to the substrate and a height and a radius equal to the average diameter and radius of the NPs, respectively. The second approximation relates to the fact that the metal coverage is not continuous. Since we are only interested in the amount of sputtered Au atoms rather than in the ejection trajectory, we take into account this fact by weighting the results obtained for a continuous Au layer by the experimentally determined coverage included in Table I.

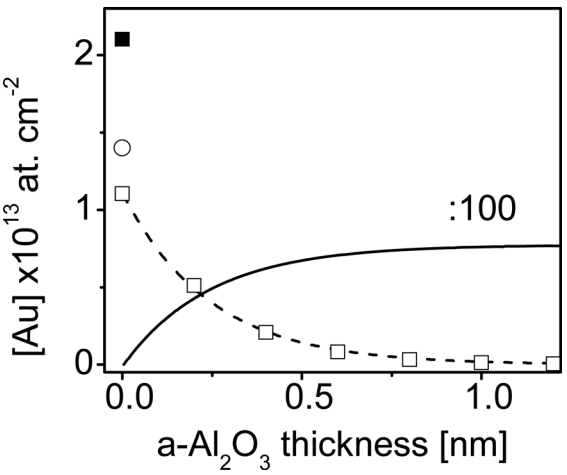

FIG. 8. Amount of Au atoms sputtered per pulse $[Au]_{SPUTT}$/pulse calculated using the SRIM-2008 code (□) (Refs. 22 and 23) and total amount of Au atoms sputtered $[Au]_{SPUTT}$ for increasing thickness of the Al_2O_3 layer deposited on top of the Au NPs of the sample prepared with 340 pulses on the gold target (solid line). The dashed line is an exponential decay fit of the calculated values. The values of $[Au]_{SPUTT}$/pulse calculated for a thickness $t = 0$ nm of Al_2O_3 using the models of Zalm (Ref. 25) (○) and Yamamura and Tawara (Ref. 26) (■) models are also included.

In order to calculate $[Au]_{SPUTT}$ from $[Au]_{SPUTT}$/pulse we must take into account that for each consecutive pulse, the thickness t of the *a*-Al_2O_3 covering layer on top of Au NPs increases and thus Al^+ ions will induce less sputtering on gold from the NPs. There will be additional self-sputtering of *a*-Al_2O_3 layer that is not considered in the present work. Consequently, $[Au]_{SPUTT}$/pulse(t) will decrease as t increases and we estimate the *a*-Al_2O_3 thickness range for which Au sputtering exists. We have considered the parameters of bulk Al_2O_3 except for the density, for which we have used the value $\rho = 2.95$ g cm^{-3} reported in literature for *a*-Al_2O_3 films produced by PLD.[31] The results for the sample in which NPs were produced using 340 pulses to ablate the gold target are shown in Fig. 8 where it is seen that an initial value $[Au]_{SPUTT}/\text{pulse}(0) = 1.1 \pm 0.4 \times 10^{13}$ atoms/cm^{-2} pulse is achieved that decreases very fast as the thickness of *a*-Al_2O_3 increases, becoming negligible above ≈1 nm.

The total amount of sputtered atoms $[Au]_{SPUTT}$ is finally calculated from the dependence shown in Fig. 8 and the experimentally measured *a*-Al_2O_3 deposition rate ($\approx 3.5 \times 10^{-3}$ nm/pulse) as

$$[Au]_{SPUTT} = \int [Au]_{SPUTT}/\text{pulse}(t)dt. \qquad \text{(A2)}$$

The results are also included in Fig. 8, where a maximum value of $[Au]_{SPUTT} = 0.8 \pm 0.3 \times 10^{15}$ atoms cm^{-2} is obtained.

As described in the text, we have also considered two other models to evaluate the extent of $[Au]_{SPUTT}$/pulse, namely the models of Zalm[25] and Yamamura and Tawara.[26]

1. Zalm's model

This model allows an analytical determination of $Y(E)$ for the case of an a-Al_2O_3 thickness of $t = 0$ using the following expression:[25]

$$Y(E) = \frac{1.9}{E_{CNP}} \left(\frac{Z_{Au}}{f}\right)^{1/2} \left(E_{Al^+}^{1/2} - 0.09 E_{CNP}^{1/2}\right). \quad \text{(A3)}$$

with

$$f = \frac{1}{2}\left[\left(\frac{Z_{Au}}{Z_{Al^+}}\right)^{2/3} + \left(\frac{Z_{Al^+}}{Z_{Au}}\right)^{2/3}\right], \quad \text{(A4)}$$

where E_{Al^+} is the projectile energy (keV), E_{CNP} is the cohesive energy (eV), Z_{Au} and Z_{Al^+} are the atomic number of Au (target) and Al^+ (projectile), respectively.

2. Yamamura and Tawara's model

The empirical formula of Yamamura and Tawara leads to $Y(E)$ values very similar to those obtained using Zalm's model and thus we have used the modification of Sigmund's formula made by Yamamura and Tawara for low-energy heavy-ion sputtering. In our case, this approximation is supported by the fact that the kinetic energy of incident Al^+ ions is in the hundreds of electron volt range, i.e., much smaller than the kiloelectron volt or even megaelectron volt involved in the standard sputtering process. However, the atomic mass of Al^+ is ≈27 and thus this calculation is in the limit of validity of the model. According to this approximation, $Y(E)$ is calculated from the following expression:

$$Y(E) = 0.042 \frac{\Theta\ \alpha^* S_n(E)}{E_{CNP}} \left[1 - \sqrt{\frac{E_{th}}{E}}\right], \quad \text{(A5)}$$

where E_{CNP} has the same meaning than before, E_{th} is the sputtering threshold energy (≈9.1 eV), $S_n(E)$ is the nuclear stopping cross section, Θ is a parameter that for the case of Au is 1.08, and finally α^* is an energy independent parameter that depends on the masses of the projectile (Al^+) and target (Au), and in our case is 0.823. The details for the calculation of $S_n(E)$ and all the other parameters can be found in the original reference.

As both models easily allow determining Y but not its dependence on a-Al_2O_3 thickness t, only the values calculated for $t = 0$ have been included in Fig. 8. The results show that both models provide higher sputtering yields than SRIM, Yamamura and Tawara's[26] leading to an increase close to a factor of 2. In order to have an estimation of the total $[Au]_{SPUTT}$ using any of these models (M) we have considered that

$$[Au]_{SPUTT}(M) = \frac{[Au]_{SPUTT}/\text{pulse}(M, 0)}{[Au]_{SPUTT}/\text{pulse}(SRIM, 0)} [Au]_{SPUTT}(SRIM), \quad \text{(A6)}$$

where $[Au]_{SPUTT}$/pulse(M, 0), and $[Au]_{SPUTT}$/pulse(SRIM, 0) stand for $[Au]_{SPUTT}$/pulse calculated using model M and SRIM-2008 software for $t = 0$, respectively. This expression corresponds to a shift of the values of $[Au]_{SPUTT}$ obtained using the SRIM-2008 software by the enhancement factor with respect to $[Au]_{SPUTT}$/pulse (SRIM-2008) obtained for $t = 0$.

[1] A. Pucci, M. Bernabo, P. Elvati, L. I. Meza, F. Galembeck, C. A. de Paula Leite, N. Tirelli, and G. J. Ruggeri, Mater. Chem. **16**, 1058 (2006).
[2] M. B. Cortie, X. Xu, and M. J. Ford, Phys. Chem. Chem. Phys. **8**, 3520 (2006).
[3] W. Rechberger, A. Hohenau, A. Leitner, J. R. Krenn, B. Lamprecht, and F. R. Aussenegg, Opt. Commun. **220**, 137 (2003).
[4] D. Tsoukalas, P. Dimitrakis, S. Kolliopoulou, and P. Normand, Mater. Sci. Eng. B **124–125**, 93 (2005).
[5] J. Requejo-Isidro, R. del Coso, J. Solis, J. Gonzalo, and C. N. Afonso, Appl. Phys. Lett. **86**, 193104 (2005).
[6] N. I. Zheludev, J. Opt. A: Pure Appl. Opt. 8, S1 (2006).
[7] Y. Takeda, O. A. Plaskin, J. Lu, and N. Kishimoto, Nucl. Instrum. Methods Phys. Res. B **242**, 194 (2006).
[8] S. Link and M. A. El-Sayed, Int. Rev. Phys. Chem. **19**, 409 (2000), and references therein.
[9] C. F. Bohren and D. R. Huffman, *Absorption and Scattering of Light by Small Particles* (Wiley, New York, 1983).
[10] U. Kreibig and M. Vollmer, *Optical Properties of Metal Clusters* (Springer, New York, 1994).
[11] S. Fähler, S. Kalh, M. Weisheit, K. Sturm, and H.-U. Krebs, Appl. Surf. Sci. **154–155**, 419 (2000).
[12] K. Sturm and H.-U. Krebs, J. Appl. Phys. **90**, 1061 (2001).
[13] J. Gonzalo, A. Perea, D. Babonneau, C. N. Afonso, N. Beer, J.-P. Barnes, A. K. Petford-Long, K. E. Hole, and P. D. Townsend, Phys. Rev. B **71**, 125420 (2005).
[14] A. Perea, J. Gonzalo, C. Budtz-Jorgensen, G. Epurescu, J. Siegel, C. N. Afonso, and J. Garcia-Lopez, J. Appl. Phys. **104**, 084912 (2008).
[15] J.-P. Barnes, N. Beer, A. K. Petford-Long, A. Suárez-García, R. Serna, D. Hole, M. Weyland, and P. A. Migdley, Nanotechnology **16**, 718 (2005).
[16] W. Rasbandl, National Institutes of Health (USA); http://rsbweb.nih.gov/ij/
[17] C. Kittel, *Introduction to Solid State Physics* (Wiley, New York, 1996).
[18] D. Xie, M. P. Wang, and W. H. Qi, J. Phys.: Condens. Matter. 16, L401 (2004).
[19] W. H. Qi, B. Y. Huang, M. P. Wang, Z. Li, and Z. M. Yu, Phys. Lett. A **370**, 494 (2007).
[20] R. W. Dreyfus, R. Nelly, and R. E. Walkup, Appl. Phys. Lett. **49**, 1478 (1986).
[21] F. Claeyssens, S. J. Henley, and M. N. R. Ashfold, J. Appl. Phys. **94**, 2203 (2003). In the course of writing this manuscript, an error has been identified in Fig. 2 related to the mean kinetic energy of Al ions as a function of fluence that corresponds to the triangles instead of the circles.
[22] P. Sigmund, Nucl. Instrum. Methods Phys. Res. B **27**, 1 (1987).
[23] J. F. Ziegler, http //www.srim.org/.
[24] K. Wittmaack, J. Appl. Phys. **96**, 2632 (2004).
[25] P. C. Zalm, J. Vac. Sci. Technol. B **2**, 151 (1984).
[26] Y. Yamamura and H. Tawara, At. Data Nucl. Data Tables, **62**, 149 (1996).
[27] G. Fuchs, P. Melinon, F. Santos Aires, M. Treilleux, B. Cabaud, and A. Hoareau, Phys. Rev. B **44**, 3926 (1991).
[28] B. Satpati, D. K. Goswami, S. Roy, T. Som, B. N. Dev, and P. V. Satyam, Nucl. Instrum. Methods Phys. Res. B **212**, 332 (2002).
[29] R. Serna, A. Suárez-García, C. N. Afonso, and D. Babonneau, Nanotechnology **17**, 4588 (2006).
[30] B. Thestrup, B. Toftmann, J. Schou, B. Doggett, J. G. Lunney, Appl. Surf. Sci. **197–198**, 175 (2002).
[31] R. Serna, J. C. G. de Sande, J. M. Ballesteros, and C. N. Afonso, J. Appl. Phys. **84**, 4509 (1998).